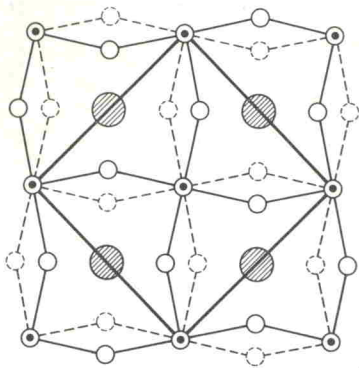


In  $ABO_3$  perovskites, distortions that optimize the anion coordination about the A cation commonly occur [8]. Although the  $Rb^+$  ion is large enough to stabilize twelfold coordination, which makes  $RbFeF_3$  cubic above  $T_N$ , a tetragonal ( $c/a > 1$ ) Jahn-Teller distortion reduces this coordination from 12 to (4 + 8). Additional distortions that would increase this coordination to (5 + 2 + 5) or (4 + 4 + 4) approaching  $(8\frac{1}{2} + 4)$  are the orthorhombic  $Pbnm$  structure of  $GdFeO_3$  [9] for the case  $c_0 \perp c_T$  and the tetragonal structure of figure 1 for the case  $c'_T = 2c_T$ . The



- $Fe^{2+}$  ion at  $z = 0, 1/2$ ;  $F^-$  ion at  $z = 1/4, 3/4$
- ◐  $Rb^+$  ion at  $z = 1/4, 3/4$
- $F^-$  ion at  $z = 0$
- $F^-$  ion at  $z = 1/2$

FIG. 1. — Tetragonal ( $c'_T = 2c_T$ ) structure projected on the (001) plane.

orthorhombic  $Pbnm$  structure (but not the tetragonal structure) permits the existence of a Dzialoshinskii vector  $\mathbf{D}$  parallel to the orthorhombic axis  $\mathbf{b}_0$ , and hence a canting of the Type G spin configuration to produce weak ferromagnetism. Thus the existence of a distortion to orthorhombic  $Pbnm$  symmetry below  $T_2$  that is superposed on a tetragonal Jahn-Teller distortion in the interval  $T_1 < T < T_N$  and a trigonal Jahn-Teller distortion below  $T_1$  provides a mechanism for the appearance of weak ferromagnetism below  $T_2$  as well as for the appearance of orthorhombic and monoclinic symmetry in the intervals  $T_1 < T < T_2$  and  $T < T_1$ , see figure 2.

Levinstein et al. [10] have demonstrated that extensive twinning takes place below  $T_N$ , indicating

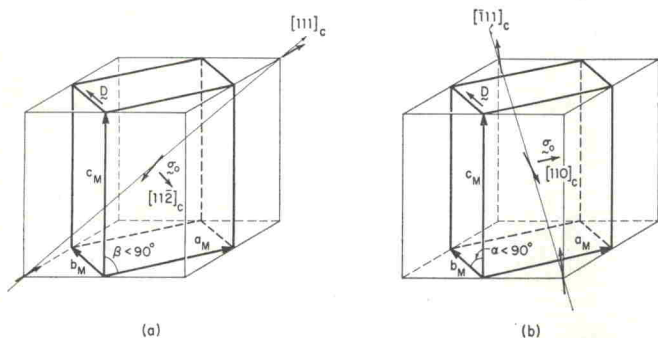


FIG. 2. — Two rhombohedral ( $\alpha < 60^\circ$ ) Jahn-Teller distortions superposed on the orthorhombic  $Pbnm$  structure: (a)  $\beta < 90^\circ$ , (b)  $\alpha < 90^\circ$ .

that strong magnetoelastic coupling is present right through  $T_N$ . This observation is compatible with dynamically cooperative Jahn-Teller distortions in regions of short-range order just above  $T_N$ , so that long-range order below  $T_N$  requires the creation of twin planes. The temperature  $T_N$  at which long-range order sets in depends upon the energy required to create twin planes for the relief of internal stresses created by the magnetoelastic coupling. In any real crystal, this energy varies from region to region, thereby leading to the spatial variation in  $T_N$  suggested by the magnetization data. Furthermore, Levinstein et al. [10] also observed directly that the ferromagnetic « orthorhombic » phase boundary moves across the twin planes of the tetragonal phase so as to include some regions having  $c_T \rightarrow \langle c_0 \rangle / 2$  and others having  $c_T \rightarrow (a_0 + b_0) / 2$ . [Although additional twinning occurs below  $T_2$ , the twin planes associated with the « orthorhombic » distortion are mobile in

$$H_a > 0.5 \text{ kOe}.$$

Therefore in an  $H_a = 5 \text{ kOe}$  (where cubic torque curves were observed [4]), magnetoelastic coupling would saturate and switch the orthorhombic component of the distortion to which  $\sigma$  is coupled, but not the twinned Jahn-Teller component to which the large, antiferromagnetic spin component is coupled. (The spins are rotated by less than  $2.5^\circ$  in an  $H_a = 16 \text{ kOe}$  [4].)

The direction and magnitude of the weak ferromagnetism in a crystal twinned by Jahn-Teller distortions but with a unique orthorhombic component can be obtained by minimizing  $\mathbf{D} \cdot \mathbf{S}_i \times \mathbf{S}_j$ . In order to obtain an [001] easy axis in the « orthorhombic » phase, it is necessary to assume that where  $c_T \rightarrow \langle c_0 \rangle / 2$ , the orthorhombic component of the distortion transforms to the tetragonal distortion of figure 1,  $c_T \rightarrow c'_T / 2$ . This simultaneously accounts for the two different hyperfine fields below  $T_2$  and, for  $H_a = 5 \text{ kOe}$  parallel to [001], leads to the weak ferromagnetism

$$\sigma^0 = (\sqrt{2/3}) [001] \sigma_0^0,$$

where the Miller indices refer to the pseudocubic cell and  $\sigma_0$  is the maximum ferromagnetism possible for the given  $\mathbf{D}$ . This clearly gives the cubic magnetic anisotropy observed. Switching of the spin axis from an [001] to a [111] direction to create the monoclinic phase, only adds a set of immobile  $\{100\}$  twin planes to the original  $\{110\}$  set. If the superposed distortions are, in this phase, everywhere orthorhombic  $Pbnm$ , then from figure 2,  $\mathbf{D} \parallel \mathbf{b}_M$  and either  $\alpha < 90^\circ$  or  $\beta < 90^\circ$ . For  $H_a = 5 \text{ kOe}$  parallel to [110], this leads to

$$\begin{aligned} \sigma^M &= \frac{1}{4\sqrt{6}} \{ [11\bar{2}] + [110] + [112] + [110] \} \sigma_0^M = \\ &= \frac{\sigma_0^M}{\sqrt{3}} \left( \frac{[110]}{\sqrt{2}} \right) \end{aligned}$$

which also gives the cubic magnetic anisotropy observed for this phase.

Significantly  $\sigma_{110}^M / \sigma_{100}^0 = \sqrt{(3/2)} \sigma_0^M / \sigma_0^0 \approx \sqrt{(3/2)}$  is in reasonable quantitative agreement with the magnetization measurements.



References

- [1] WERTHEIM (G.), GUGGENHEIM (H.), WILLIAMS (H.) and BUCHANAN (D.), *Phys. Rev.*, 1967, **158**, 446.
- [2] TESTARDI (L.), LEVINSTEIN (H.) and GUGGENHEIM (H.), *Phys. Rev. Letters*, 1967, **19**, 503.
- [3] WANG (F.) and KESTIGIAN (M.), *J. Appl. Phys.*, 1966, **37**, 975.
- [4] GYORGY (E.), LEVINSTEIN (H.), DILLON, JR. (J.) and GUGGENHEIM (H.), *J. Appl. Phys.*, 1969, **40**, 1599.
- [5] WANG (F.), COX (D.) and KESTIGIAN (M.), *Bull. Am. Phys. Soc.*, 1968, **13**, 468.
- [6] MENYUK (N.), KAFALAS (J.), DWIGHT (K.) and GOODENOUGH (J.), *J. Appl. Phys.*, 1969, **40**, 1324.
- [7] GOODENOUGH (J.), *Phys. Rev.*, 1968, **171**, 466.
- [8] GELLER (S.), *J. Chem. Phys.*, 1956, **24**, 1236.
- [9] GOODENOUGH (J.) and LONGO (J.), Landolt-Bornstein Tabellen, Neue Serie III/4 a (1970, Springer-Verlag, Berlin), 126.
- [10] LEVINSTEIN (H.), GUGGENHEIM (H.) and CAPIO (C.), *Trans. A. I. M. E.*, 1969, **245**, 365.

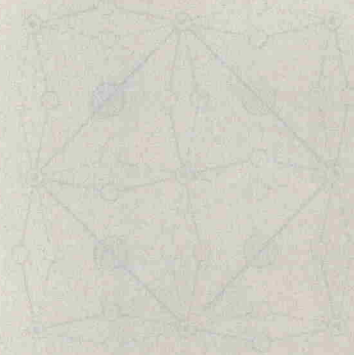


Fig. 1. Crystal structure of the perovskite phase. The central atom is shown in blue, and the oxygen atoms are shown in red. The structure is based on a cubic lattice.

The crystal structure of the perovskite phase is based on a cubic lattice. The central atom is shown in blue, and the oxygen atoms are shown in red. The structure is based on a cubic lattice.



Fig. 2. Crystal structure of the layered phase. The structure is based on a cubic lattice.